JTTEE5 17:525–532
DOI: 10.1007/s11666-008-9205-1
1059-9630/$19.00 © ASM International

Fatigue Behavior of Bodies with Thermally Sprayed Metallic and Ceramic Deposits

Ondřej Kovářík, Jan Siegl, and Zdeněk Procházka

(Submitted October 24, 2007; in revised form February 4, 2008)

This paper summarizes the basic results of fatigue testing of bodies with both metallic and ceramic thermally sprayed coatings. Three kinds of ceramic coatings (Al_2O_3, Cr_2O_3, and olivine) sprayed with DC plasma under identical conditions were investigated together with metallic Ni-5wt.%Al coatings sprayed by wire arc, DC plasma, and HVOF. The elastic modulus of the deposited coatings was investigated using four point bending and resonance method. Bending fatigue tests at resonance frequency were performed with cantilever beam specimens. The processes taking place during the fatigue test are identified and discussed. The morphology of the fracture surfaces was investigated together with microstructure and porosity of the coatings.

Keywords elastic modulus, fatigue, fractography, residual stress, thermally sprayed coatings

1. Introduction

The most sensitive part of any component from the point of view of fatigue failure is its surface. The surface sensitivity to crack initiation is further enhanced by other forms of surface degradation (caused by loading and/or environmental action). Therefore, the surface properties considerably restrict the usage of classical engineering materials for high-performance applications. Thermally sprayed coatings and other surface modifications are often used to increase component lifetime by preventing surface degradation processes (Ref 1). The thermally sprayed coatings are built of individual splats of different flattening degrees, unmelted powder particles, in-flight resolidified feedstock particles, small 'debris' particles resulting from splashing of individual splats at the point of impact, and other features, all of that separated by a porosity network. This complicated nature of thermally sprayed coatings leads to significant differences in mechanical, thermal and fatigue properties compared to bulk material of the same chemical composition (Ref 2-5). Also, the mechanical properties of the substrate material are often significantly changed before and during the deposition process as a result of sample preparation before spraying and/or the thermal and mechanical loading of the substrate during coating deposition.

Ondřej Kovářík and **Jan Siegl**, Department of Materials, Faculty of Nuclear Sciences and Physical Engineering, Czech Technical University in Prague, Trojanova 13, 120 00 Praha 2, Czech Republic; and **Zdeněk Procházka**, Office of Research, Nanyang Technological University, 50 Nanyang Avenue, Blk N4, B4b-09, Singapore, Singapore 639798. Contact e-mails: kovon@seznam.cz and kovarik@kmat.fjfi.cvut.cz.

The deposit can influence the fatigue properties of coated part in two principal ways. Hard deposits often show lower than bulk properties due to microcracking of brittle splats. Thus, during fatigue loading the network of small cracks may form or the branching of main fatigue crack may appear in the coating (Ref 6). In this way, the deposit can accommodate the deformation without allowing a major crack to enter the coating/substrate interface. The major fatigue crack then initiates on the substrate surface close to large pores, abrasive particles entrapped by grit-blasting, cracks formed during deposition, etc. The crack initiation can be further inhibited by constraining the local plastic deformation by hard deposit as described in (Ref 7). Such mechanism requires dense deposit at least neat the interface and good adherence between the coating and substrate (Ref 7).

For softer deposits, near-bulk properties can often be achieved, and considerable residual stresses may develop as a result of particle quenching and deposit cooling. The crack initiation sites can be either in the substrate or in the deposit, depending on the fracture toughness, presence and effectivity of stress concentration centers, and residual stress. Compressive stress can inhibit crack initiation and propagation and prolong fatigue life (Ref 7-10). On the other hand, tensile stress will shorten the fatigue life. The first layer of splats deposited on the substrate makes things more complicated; its residual stress can be different from the rest of the deposit (Ref 11) and may well control the crack initiation in the substrate or act as a crack barrier for cracks propagating from the deposit. Thus, the fatigue resistance of bodies with deposits can be correlated to multiple factors such as residuals stresses at different parts of the deposit, deposit elastic modulus, microstructure, fracture toughness. The properties and characteristics of certain deposits can be found in the literature (Ref 4, 5, 12). Some of these deposits were chosen for the present investigation. Alumina, chromia, and olivine sprayed with water-stabilized DC plasma represent ceramics. The alloy Ni-5wt.%Al sprayed by wire arc, DC plasma, and HVOF

represents metals. The fatigue tests in symmetric bending at resonance frequency were performed to obtain samples for fractographic analysis and to estimate statistical significance of deposit influence on fatigue life. Due to limited specimen numbers, all fatigue tests were performed under the same deflection of the free end of the cantilever specimen.

2. Experimental

Fatigue tests of thermally sprayed bodies followed by subsequent fractographic analysis of the failed specimens were conducted. Reference specimens (R) without any surface modification and grit-blasted specimens (GB) without coating were also tested.

2.1 Test Specimens

The test specimens were made of a 4 mm thick low carbon steel sheet. The final shape and dimensions of specimens are shown in Fig. 1. All coatings were applied on both faces of the specimens immediately after grit-blasting. The symmetry of the specimens ensures that no specimen bending occurs; thus, no bending-induced stress gradient is present in the specimen.

Chromia (Cr_2O_3), alumina (Al_2O_3), and olivine ($(Mg, Fe)_2SiO_4$) coatings deposited using water-stabilized plasma system WSP® PAL 160 were selected for the study of the feedstock influence. Metallic Ni-5wt.%Al coatings for spray technology influence investigation were deposited at the State University of New York at Stony Brook (SUNY) using similar conditions as in (Ref 5). The particle size was around 45 μm for all feedstock powders. In total, 96 specimens grouped to 8 sets were prepared. Individual sets were denoted as described in Table 1.

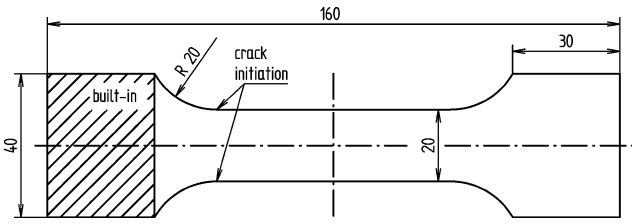

Fig. 1 The shape and dimensions of test specimens (4 mm thickness). Arrows indicate crack initiation sites

Table 1 The overview of tested specimen sets

Set	Feedstock	Grit-blast	Torch	h_c, mm	Number
R	…	…	…	…	14
GB	…	Yes	…	…	28
Al	Al_2O_3	Yes	WSP(a)	0.4, 0.8, 0.9	18
Ol	Olivine	Yes	WSP	0.7, 1.3	12
Cr	Cr_2O_3	Yes	WSP	0.5	6
NiWA	Ni-5wt.%Al	Yes	Wire Arc(b)	0.4	6
NiPS	Ni-5wt.%Al	Yes	APS(c)	0.4	6
NiHV	Ni-5wt.%Al	Yes	HVOF(d)	0.4	6

(a) WSP® PAL 160, z_s = 350 mm
(b) Tafa 8830, z_s = 175 mm
(c) Metco 3MB, z_s = 100 mm
(d) SM DJ2700, z_s = 230 mm

2.2 Fatigue Tests

Fatigue tests were carried out on an electromagnetic computer controlled testing device "SF-Test," Fig. 2. The flat specimens were loaded by symmetrical cyclical bending (as cantilever beams) with constant free-end deflection amplitude u at room temperature and with the loading frequency corresponding to the first natural frequency f of the mounted specimens (70 ÷ 100) Hz. The excitation frequency was maintained using phase locked loop technique.

A typical development of the resonance frequency f_r in course of the fatigue life is shown in Fig. 3, together with the temperature development in the crack initiation area (see Fig. 1) measured by a thermocouple spot-welded to the specimen. Similar temperature development curves can be found in literature, i.e., (Ref 13). At the beginning of the experiment, the heat dissipated by the internal

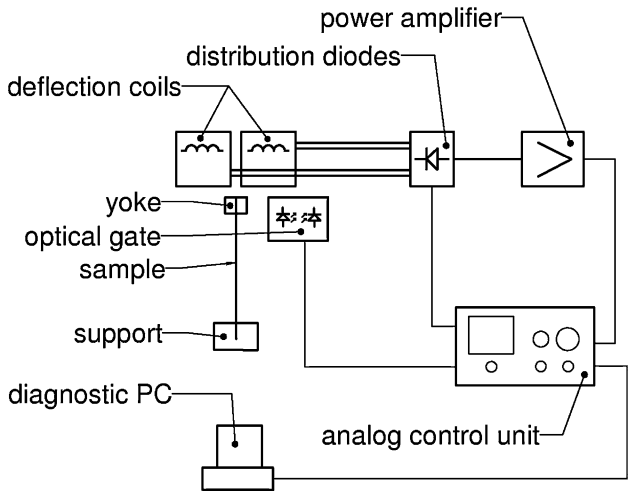

Fig. 2 Fatigue testing device SF-Test and its schematic diagram

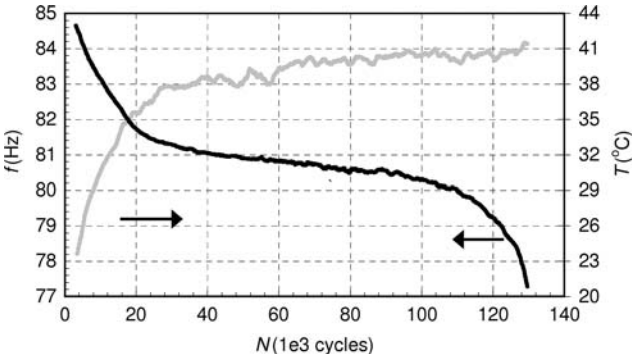

Fig. 3 Typical frequency and temperature history of the specimen

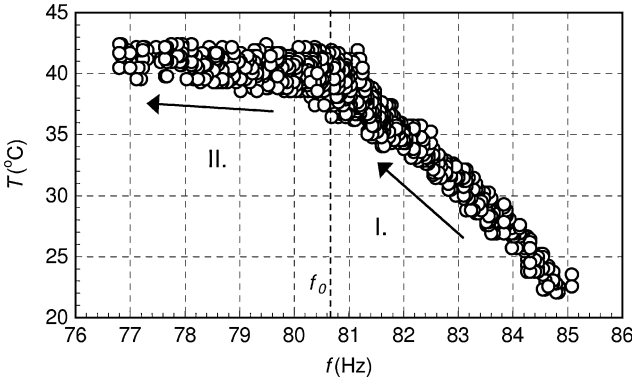

Fig. 4 Typical sample temperature and frequency development during fatigue test. Arrows show the course of the fatigue experiment

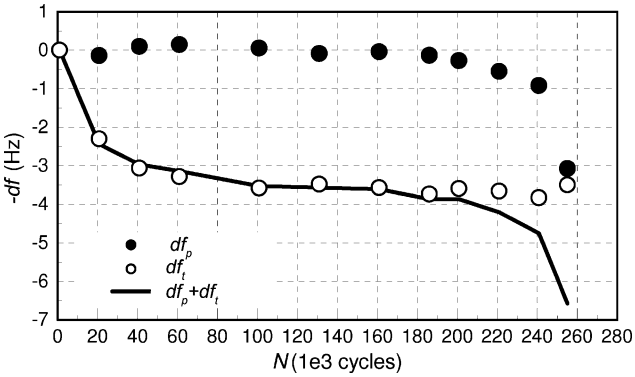

Fig. 5 Permanent and transient part of frequency change of a typical specimen

friction of the material increases the temperature of the specimen up to the point when sufficient thermal gradient is established and steady state heat transfer reached. Plotting temperature versus frequency provides another overview of the events taking place (see Fig. 4).

The correlation between temperature and frequency in the first half of the experiment (see Fig. 4, part I) may suggest that the increase of specimen temperature caused by internal friction is the cause of the frequency change. However, elevated temperature (up to 150 °C) testing of selected specimens did not support this hypothesis. The temperature increase and simultaneous frequency decrease in the first half of the experiment are indicators of material property changes. Let $df = f(0) - f$ be the frequency decrease from the starting frequency $f(0)$. The frequency decrease df is a sum of the transient part df_t and the permanent part df_p. The transient part is likely caused by transient cyclic softening of the substrate, and the permanent part is caused by compliance loss due to cracking. If the experiment is paused and resumed, the transient part disappears and pure permanent part remains, so $df = df_p$. Before the pause both permanent and transient parts are present, so $df = df_p + df_t$. The values of df_p and df_t estimated from the fatigue test data (test interrupted approx. every 20,000 cycles) are included on Fig. 5. In the first half of the experiment the frequency decrease is transient, whereas permanent frequency changes are added in the second half. In the second half of the experiment, the df_t is constant approximated by $df_t \cong f(0) - f(N/2)$, thus $df_p \cong f - f(N/2)$; where N is the fatigue life length. The assumption enables the estimation of df_p without test interruption. Following the above discussion, crack area size can be estimated as a function of df_p.

For selected plain steel specimens, the fatigue test was stopped several times and the crack areas were estimated. The lengths of the crack mouths were measured by an optical microscope. Under the assumption of quarterellipse or halfellipse crack shapes, the crack area could be estimated. The total crack area A follows linear relationship with the frequency decrease df_p. The following formula was obtained by least squares approximation: $\frac{A}{A_0} \cong 0.1(f(N/2) - f)$, where f is in Hz and A_0 is the

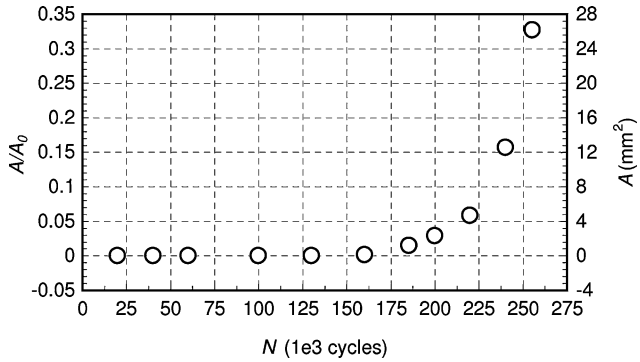

Fig. 6 Crack area development with the number of cycles

cross-sectional area of the specimen (80 mm^2). A typical crack area versus the number of cycles is plotted in Fig. 6. The frequency change $f(N/2) - f = 4$ Hz was used as a stopping condition to obtain approx. 40% of specimen cross-sectional damage.

The surface treatment influence on the fatigue life is characterized by the relative fatigue life R_f, defined as the proportion of the mean fatigue life of the set with given surface treatment to the mean fatigue life of the reference set (i.e., $R_f = 1$ corresponds to the relative fatigue life of specimens without any surface treatment). Although the relative fatigue lives may differ for different loading amplitudes (deflections of free end), the tests were only performed for single amplitude due to limited number of available specimens.

The amplitude u of free-end deflection was selected as follows. The longitudinal loading stress at the crack initiation area of the uncoated specimen was computed by FEM code as $\sigma_y \cong E * u/4$. For coated specimens, the substrate deflection will be the same; thus the loading stress will be identical. However, residual stresses will add to the loading stress as discussed in the introduction, and so the total stress field acting in the specimen will be different from that in the uncoated specimen. Thus, the loading well above the fatigue limit ensures sample fracture and reasonable test time.

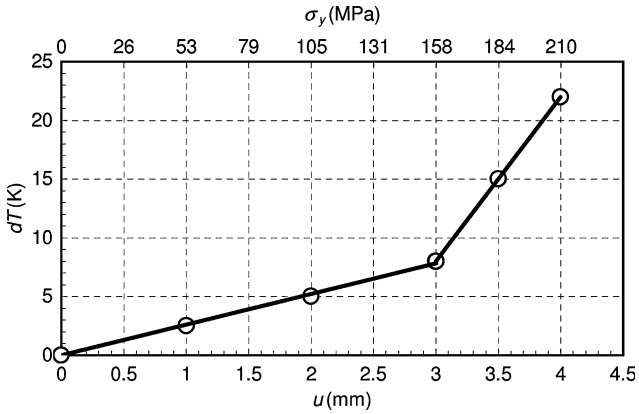

Fig. 7 Steady state temperature (relative to room temperature) versus the deflection of the free end

Table 2 The results of the fatigue tests

Set	$f(0)$, Hz	$f(N/2)$, Hz	$f(0) - f(N/2)$, Hz	R_f, 1	N, 1
R	73.6	71.6	2	1	348,000
GB	72.7	71.6	1.0	1	350,000
Al	76.3	75.2	1.1	1.9	662,000
Ol	75.1	74.2	0.9	3	104,2000
Cr	78.3	76.5	1.8	2.7	938,000
NiPS	81.5	78.9	2.6	0.15	52,000
NiWA	75.4	72.3	3.2	0.24	84,000
NiHV	103.5	99.4	4.1	2.3	800,000

The fatigue limit was estimated using the method from [14]. The measured relationship of sample temperature and free-end deflection shown in Fig. 7 suggests that the fatigue limit is reached at approximately 3 mm deflection. For $d = 3$ mm, the loading stress is around 160 MPa in crack initiation area (shown in Fig. 1). Deflection $d = 4$ mm ($\sigma_y = 210$ MPa) was selected for testing to ensure that the substrate loading will be above the fatigue limit even for coated specimens with high residual stresses.

The frequency characteristics, together with average fatigue life of specimens from different, sets are presented in Table 2. For sets containing multiple coating thicknesses, the average value is used. Results of statistical tests concerning the influence of coating thickness on fatigue life justified this approach.

2.3 Elastic Modulus

The elastic moduli of metallic coatings were taken from (Ref 5) where the same feedstock and similar spray conditions were used. For ceramic specimens, the elastic modulus of the coatings was roughly estimated from the resonance frequency at the mid-fatigue life f_0 and the mass of the specimen. The parameters A and B of a single degree of freedom oscillator were evaluated by FEM code. Using average sample density ρ_{cz} (estimated from sample weight and deposit thickness, and can be used to estimate total porosity of deposit) and resonance frequency f_0, the modulus of the substrate-coating composite beam was computed as $E_{cs} = (\rho_{cs} + B)(A/f_0)^{-2}$.

Table 3 Elastic modulus (four point bending) and residual stress (neutron data from (Ref 12))

Set	E, GPa	Total porosity, %	$\sigma_{substrate\ interface}$, MPa	$\sigma_{coating}$	
				Interface, MPa	Surface, MPa
R	…	…	−28 ± 3(a)	…	…
GB	…	…	−145 ± 9(a)	…	…
Al	43 ± 15	28 ± 3	−40	23	27
Ol	32 ± 4(c)	30 ± 5	…	…	…
Cr	43 ± 5(c)	18 ± 4	…	…	−4(a)
NiPS	78 ± 6	20.5(b)	−133	18	318
NiWA	103 ± 25	16.5(b)	5	−332	198
NiHV	166 ± 5	3.1(b)	463	−674	−636

(a) XRD stress
(b) Porosity and oxide contents from (Ref 5)
(c) Resonance modulus

The coating modulus was then extracted from the composite modulus using a momentum balance in pure uniaxial bending as:

$$E_c = \frac{E_{cs} - E_s}{\left(\frac{H}{2} + h\right)^3 - \left(\frac{H}{2}\right)^3} \left(\frac{H}{2}\right)^3$$

where E_c and E_s is the coating and substrate elastic modulus, respectively, and h and H is the coating and substrate thickness, respectively. The Elastic moduli are included in Table 3.

2.4 Residual Stress

The residual stresses of single side coated specimens—2.5 mm substrate thickness with 1.9 mm coating—measured by neutron diffraction were taken from (Ref 12). The deformation stresses induced by specimen bending were subtracted from the stress data under the assumption of a linear elastic behavior of the substrate and coating and considering the elastic modulus of deposit given in Table 3. Although the magnitude of the stresses will differ from the investigated thin coatings, the included data provide valuable qualitative description of the substrate/coating residual stress field.

For some ceramic coating and also for grit-blasted specimen, XRD measurement data are available from (Ref 10) and (Ref 15). For XRD measurements, stresses in longitudinal dimension of the specimens are presented. Such measurements correspond qualitatively with available transformed neutron data.

2.5 Fractography

To access the fracture surfaces, the fatigued specimens were ruptured on a tensile test machine. The micromorphology of fracture surfaces of both the coating and the substrate was observed using JEOL JSM-5510LV scanning electron microscope (SEM) working in backscattered shadow mode (off-axis detector was used to visualize the micromorphology). Nonconductive ceramic coatings were observed in low-vacuum mode. The fractographic analysis

provides information about the coating microstructure as well as about the failure mechanism of the coating and substrate.

3. Results

The results of fatigue tests are presented in Table 2 and Fig. 8, and the elastic modulus of and the residual stress in the coating and substrate is in Table 3.

The fatigue test results (Table 2) clearly showed that grit-blasting by itself must not necessarily lead to significant changes in fatigue behavior. Grit-blasting of the substrate introduces several effects such as surface roughness, compressive residual stress field (see XRD stress in Table 3), surface hardening, arrest of blasting particles (Ref 16). The residual stress at the substrate surface increases its magnitude significantly after grit-blasting as compared to as-received state (set R in Table 3). Surface roughness and grit residue act as stress concentrators assisting fatigue cracks initiation. Work hardening together with compressive residual stress on the other hand acts against fatigue crack initiation and propagation. In the present experiments, the effects cancelled out and so no statistically important change of fatigue life due to grit-blasting was detected.

The graph in Fig. 8 unambiguously proves that all types of investigated coatings have significant influence on fatigue behavior. All three investigated ceramic coatings showed significant fatigue life increase (more than 1.9 times). The influence of Ni-5wt.%Al coatings was more complicated. While HVOF-sprayed Ni-5wt.%Al coatings led to twofold fatigue life increase, the plasma and/or wire arc-sprayed Ni-5wt.%Al coatings decreased fatigue lives of investigated specimens more than four times.

For metallic deposits, elastic modulus follows opposite trend to porosity (see Table 2 and 3). This is rather common finding (see, i.e., Ref 2, 5), as the presence of pores decreases the compliance of the deposit. The elastic modulus of the deposit together with other factors influences the residual stress. For linear elastic materials, the thermal stresses are proportional to the modulus of the deposit. Also, the primary quenching is less released by deposit deformation if the modulus of the deposit is high. It was observed that the transient frequency change $df_t(N/2) \cong f(0) - f(N/2)$ follows the same trend as elastic modulus (see Table 2). Probably this frequency decrease is caused by transient softening of both the deposit and the substrate. This transient softening follows work hardening and residual stress formation during spraying. The ceramic coatings show lower value of $df_t(N/2)$ as limited plastic deformation occurs in the brittle ceramic coating, lower residual stresses are present, and the modulus of the deposit is low.

The fractographic findings of failed specimens confirmed our previous results (see, e.g., Ref 4). The thermally sprayed coatings do not influence the fatigue failure mechanism of the substrate (low carbon steel sheet). Fatigue cracks in the substrate initiate either on specimen edges or on faces and grow by striation mechanism as 1/4 or 1/2 elliptical cracks. The fracture micromorphology of the coating is predetermined by its microstructure. The coatings failed by mechanisms of intrasplat cracking and/or intersplat decohesion (see micrographs of all investigated coatings in Fig. 9 and 10). In contrast to the substrate, the fractures of the deposit do not provide unambiguous fractographic features necessary for the location of the crack initiation site or for the determination of the crack propagation directions.

Micrographs in Fig. 9a-c illustrate the influence of feedstock materials on fracture micromorphology of

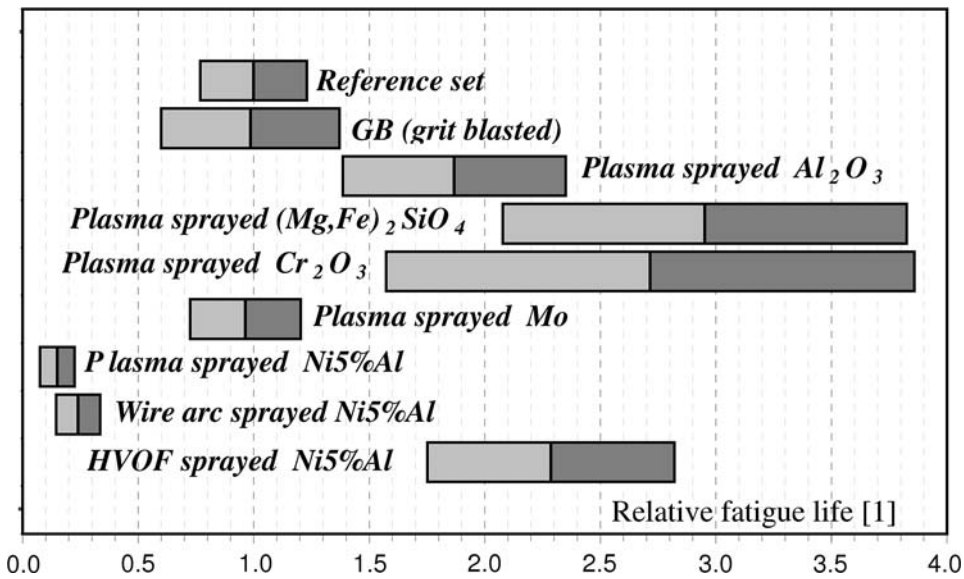

Fig. 8 Results of fatigue tests—the bars represent standard deviation, and the average value is between bars

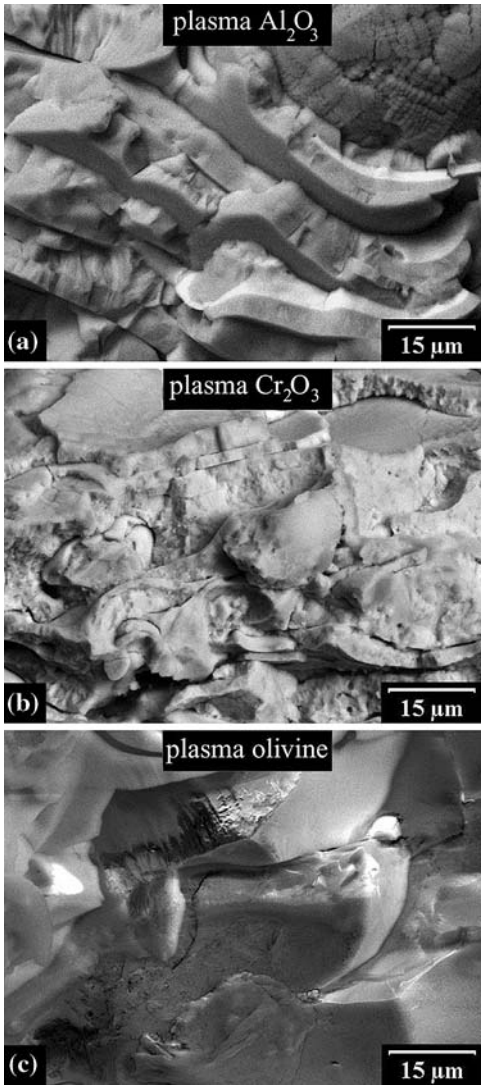

Fig. 9 Fracture morphology of ceramic coatings

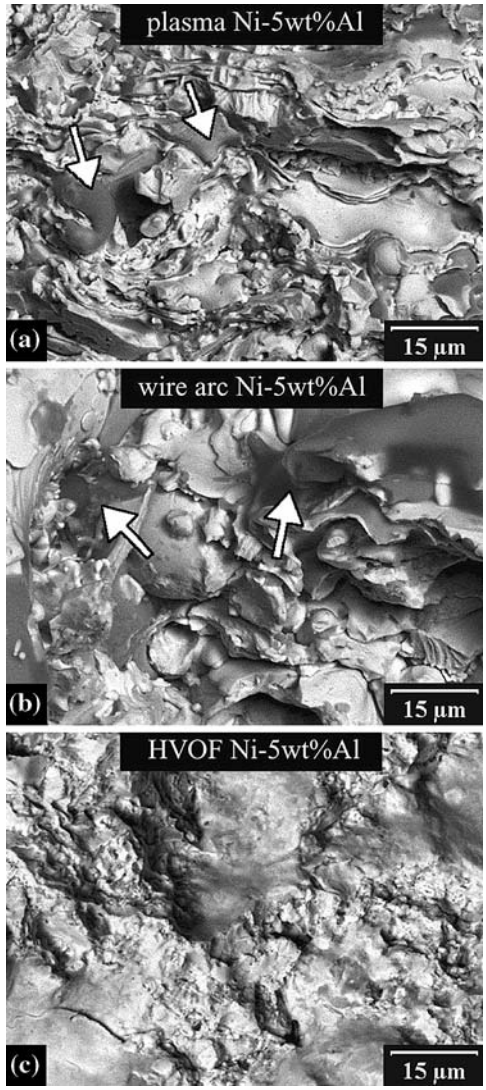

Fig. 10 Fracture morphology of metallic coatings; arrows on images (a) and (b) indicate oxide particles

ceramic coatings. Fractures of alumina and chromia coatings are very similar. The cracks are formed by intrasplat cracking and intersplat decohesion. The intrasplat cracking is promoted by high splat flattening ratio. Occasionally spherical particles (either unmelted or resolidified) are found (Fig. 9a). The smaller flattening ratio of splats in olivine coatings leads to higher occurrence of intersplat decohesion (Fig. 9c). The presence of intrasplat cracks was rare. The fatigue cracks originated near the specimen edges, i.e., in areas with natural stress concentration (see. Fig. 11b), and maintained its plane of propagation during crack growth. Crack initiations on the faces of the specimens were rarely observed.

Micrographs in Fig. 10a-c illustrate the influence of spray technology on fracture micromorphology of metallic Ni-5wt.%Al coatings. For all deposits, most of the fracture surface was formed by intersplat decohesion. The decohesion occurs namely for splats with inclined orientation. Fractures of coatings produced using APS show splats with high flattening ratio (Fig. 10a) and common oxide layers between splats (arrows on Fig. 10a). Fractures of wire arc-sprayed coatings are characterized by larger irregular splats with oxide layers between splats (Fig. 10b). The EDX analysis confirmed the results of (Ref 5) that the oxide layers are formed mainly by Al_2O_3. Only few pores and no oxide particles were observed in HVOF-sprayed deposits due to low in-flight particle temperature and short residence time. With some difficulties, the evidence of deposit abrasion invoked by cyclic crack opening and closing was identified in the HVOF deposit. Such a finding suggests that the fracture of the part of deposit adjacent to the fatigue crack in the substrate appeared before the final specimen rupture performed in the tensile machine (to access fracture surfaces).

The analysis of the obtained data (Table 3) shows that, for metallic materials, the compressive residual stress in

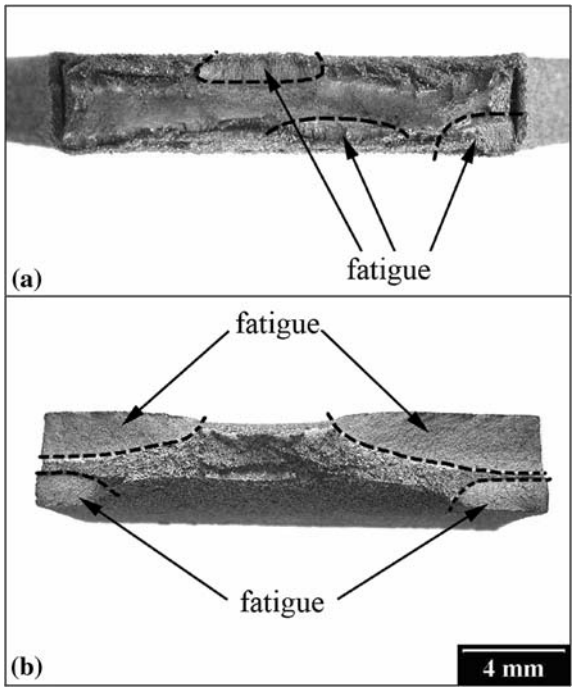

Fig. 11 Typical fatigue crack shapes in the substrate. (a) Crack initiation on the face of specimen ($R_f < 1$, Ni-5wt.%Al, wire arc) and (b) crack initiation on the substrate edge ($R_f \geq 1$, no deposit)

deposit leads to an increased fatigue life (HVOF deposit). The compressive stress of HVOF deposit is given by the combination of peening action (fast spray particles) and low quenching stress (cold spray particles). Similar effect of compressive deposit stress was observed, in (Ref 8) for WC-Co on Aluminum. Fatigue life improvement was indicated in (Ref 9) for HVOF-coated WC-Co specimens with tensile residual stress in the deposit. Tensile residual stress combined with higher deposit porosity (see Table 3 and Ref 5) on the other hand led to fatigue life decrease (plasma, wire-arc). Two types of crack initiation in the substrate were observed (see Fig. 11). The substrate crack originated at the natural stress concentrator at the specimen edge for specimens with $R_f \geq 1$ (HVOF). On the other hand for $R_f < 1$, the crack initiation sites are predetermined by the nonhomogeneity of the deposit and substrate resulting in stress concentration at the faces of the specimen. This above discussion supports the hypothesis that, in metal deposits, the fatigue cracks initiated at the surface of the deposit and consequently grew into the substrate.

The measured residual stress in samples with alumina deposits is very low, due to low elastic modulus of the deposit and quenching stress relaxation by splat cracking. Thus, the residual stress field cannot explain the fatigue behavior of alumina-coated specimens. It is possible that hard ceramic coating can block localized plastic deformation on the substrate surface and thus inhibit crack initiation in deposit as described in (Ref 7). The fact that the hardness of the ceramic deposits is much higher (1500 HV) than the hardness of Ni5%Al (120-368 HV (Ref 17)) supports the hypothesis.

4. Conclusion

The influence of thermally sprayed coatings on fatigue behavior of ''composites'' coating-substrate was studied. The objective of determining the effect of thermally sprayed coatings on fatigue life was accomplished by the constant deflection symmetrical bending test. The influence of various surface treatments on fatigue lives can be summarized as follows:

(a) Effect of grit-blasting on fatigue life was statistically insignificant. The influence of compressive stresses originating from grit-blasting was compensated by the creation of micronotches on specimen surface.

(b) The application of thermally sprayed coatings significantly changed the mean fatigue life of the tested specimens with coatings compared to the fatigue lives of specimens without coating.

(c) All specimens with ceramic coatings (alumina, chromia, and olivine) lead to longer fatigue lives when compared to specimens without coating.

(d) Fatigue lives of sets with metallic coatings depended significantly on the spraying technique; both increase and decrease of the mean fatigue life was noticed.

(e) Correlation between fatigue life length and residual stress, elastic modulus, and porosity was detected for specimens with metallic coatings. Unfortunately, all three factors changed between different specimen sets; thus, effects of individual factors could not be estimated.

The influence of spray technology for metallic deposits and feedstock material for ceramic deposits can be summarized as follows:

Spray technology influence: The properties of the deposit and consequently the fatigue lives of sets with Ni-5wt.%Al metallic coatings strongly depend on the used spraying technique. The differences in deposition processes resulting in different particle temperatures and velocities at the point of impact lead to considerable differences in microstructure, mechanical properties, residual stress field, and fatigue performance of the deposits.

Feedstock material influence: All three ceramic coatings were deposited using identical water-stabilized plasma spray torch operated under similar conditions. Although the microstructures and hence the fracture morphologies of the deposits are different, all ceramic specimens exhibit similar increase of fatigue life (as tested by Wilcoxon nonparametric test).

Acknowledgments

This research has been supported by Czech Science Foundation grant No. 106/05/0483. CTSR of SUNY at Stony Brook is acknowledged for specimen preparation.

References

1. S. Sampath and R. McCune, Thermal-Spray Processing of Materials, *MRS Bull.*, 2000, **25**(7), p 12-14
2. O. Kovářík, J. Bensch, G. Massini, M. Boulos, and X. Fan, Induction Plasma Deposition of Refractory Metal: Processing Parameters Optimization, *International Thermal Spray Conference 2007: Global Coating Solution*, B.R. Marple, M.M. Hyland, Y.C. Lau, C.J. Li, R.S. Lima, and G. Montavon, Eds., ASM International, Beijing, China, 2007, p. 727-732
3. A. Vaidya, T. Streibl, L. Li, S. Sampath, O. Kovářík, and R. Greenlaw, An Integrated Study of Thermal Spray Process-Structure-Property Correlations: A Case Study for Plasma Sprayed Molybdenum Coatings, *Mat. Sci. Eng. A-Struct.*, 2005, **403**(1-2), p 191-204
4. O. Kovářík, J. Siegl, J. Nohava, and P. Chráska, Young's Modulus and Fatigue Behaviour of Plasma Sprayed Alumina Coatings, *J. Therm. Spray Technol.*, 2005, **14**(2), p 231-238
5. S. Sampath, X.Y. Jiang, J. Matejicek, L. Prchlik, A. Kulkarni, and A. Vaidya, Role of Thermal Spray Processing Method on the Microstructure, Residual Stress and Properties of Coatings: An Integrated Study for Ni-5 wt%Al Bond Coats, *Mat. Sci. Eng. A-Struct.*, 2004, **364**(1–2), p 216-231
6. D.M. Zhu and R.A. Miller, Investigation of Thermal High Cycle and Low Cycle Fatigue Mechanisms of Thick Thermal Barrier Coatings, *Mat. Sci. Eng. A-Struct.*, 1998, **245**(2), p 212-223
7. M.R. Stoudt, R.E. Ricker, and R.C. Cammarata, The Influence of a Multilayered Metallic Coating on Fatigue Crack Nucleation, *Int. J. Fatigue*, 2001, **23**, p S215-S223
8. A. Ibrahim and C.C. Berndt, The Effect of High-Velocity Oxygen Fuel, Thermally Sprayed WC-Co Coatings on the High-Cycle Fatigue of Aluminium Alloy and Steel, *J. Mater. Sci.*, 1998, **33**(12), p 3095-3100
9. R.T.R. McGrann, D.J. Greving, J.R. Shadley, E.F. Rybicki, T.L. Kruecke, and B.E. Bodger, The Effect of Coating Residual Stress on the Fatigue Life of Thermal Spray-Coated Steel and Aluminum, *Surf. Coat. Tech.*, 1998, **109**(1–3), p 59-64
10. A. Ibrahim and C.C. Berndt, Fatigue and Deformation of HVOF Sprayed WC-Co Coatings and Hard Chrome Plating, *Mat. Sci. Eng. A-Struct.*, 2007, **456**(1–2), p 114-119
11. J. Matejicek and S. Sampath, Intrinsic Residual Stresses in Single Splats Produced by Thermal Spray Processes, *Acta Mater.*, 2001, **49**(11), p 1993-1999
12. O. Kesler, J. Matejicek, S. Sampath, S. Suresh, T. Gnaeupel-Herold, P.C. Brand, and H.J. Prask, Measurement of Residual Stress in Plasma-Sprayed Metallic, Ceramic and Composite Coatings, *Mat. Sci. Eng. A-Struct.*, 1998, **257**(2), p 215-224
13. H.T. Lee, J.C. Chen, and J.M. Wang, Thermomechanical Behavior of Metals in Cyclic Loading, *J. Mater. Sci.*, 1993, **28**(20), p 5500-5507
14. M.P. Luong, Fatigue Limit Evaluation of Metals Using an Infrared Thermographic Technique, *Mech. Mater.*, 1998, **28**(1–4), p 155-163
15. J. Dubský, B. Kolman, and M. Vyšohlíd, Residual Stresses and Young-modulus of Alumina and Chromia Plasma Sprayed Deposits, *United Thermal Spray Conference UTSC 99*, E. Lugscheider and P.A. Kammer, Eds., D.V.S-Verlag, Düsseldorf, Germany, 1999, p. 659-663
16. M. Mellali, A. Grimaud, A.C. Leger, P. Fauchais, and J. Lu, Alumina Grit Blasting Parameters for Surface Preparation in the Plasma Spraying Operation, *J. Therm. Spray Technol.*, 1997, **6**(2), p 217-227
17. L. Prchlik and S. Sampath, Effect of the Microstructure of Thermally Sprayed Coatings on Friction and Wear Response Under Lubricated and Dry Sliding Conditions, *Wear*, 2007, **262**(1–2), p 11-23